Received: 29 October 2020 | Revised: 21 March 2021 | Accepted: 22 March 2021

DOI: 10.1002/ppap.202000223

COMMUNICATION

PLASMA PROCESSES AND POLYMERS

Investigation of NH_4NO_3 formation by air plasma and wasted ammonia

Yu Zhu | **Zilan Xiong** | **Mengqi Li** | **Xingyu Chen** | **Chen Lu** | **Zhenping Zou**

State Key Laboratory of Advanced Electromagnetic Engineering and Technology, Huazhong University of Science and Technology, Wuhan, Hubei, China

Correspondence
Zilan Xiong, State Key Laboratory of Advanced Electromagnetic Engineering and Technology, Huazhong University of Science and Technology, Wuhan, 430074 Hubei, China.
Email: zilanxiong@hust.edu.cn

Funding information
Independent Innovation Fund of Huazhong University of Science and Technology, Grant/Award Number: 2018KFYYXJJ071

Abstract

This study investigated NH_4NO_3 formation by air plasma and NH_3 in three different reaction modes for nitrogen fixation and environmental protection. A DC-driven needle–needle discharge was used. We found that NH_4NO_3 could be effectively formed by directly mixing NO_x (generated by air discharge) and NH_3 in Mode 1. In Mode 3, when discharging in the air/NH_3 mixture, no NH_4NO_3 was detected. However, in Mode 2, when discharging in the NO_x/air/NH_3 mixture, NH_4NO_3 was first formed and then subsequently decreased as the discharging time increased. NH_4NO_3 was identified by white smoke observation and gas/aqueous-phase Fourier-transform infrared spectroscopy (FTIR) analysis. Stable NH_4NO_3 formation may be affected by self-thermal decomposition and NH_3 decomposition through discharge.

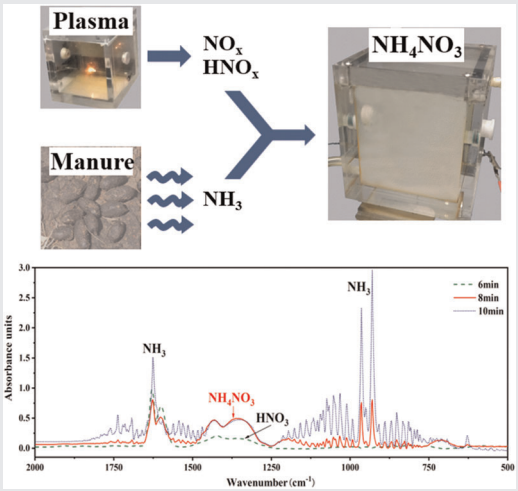

KEYWORDS
air plasma, environmental protection, NH_4NO_3, nitrogen fixation, wasted ammonia

INTRODUCTION

Nitrogen fertilizer is an essential nutrient for plant growth on earth. Modern nitrogen fertilizer production is mainly through the Haber–Bosch process in chemical fertilizer plants, which are reported to consume 1%–2% of global energy and emit roughly 1% of global annual CO_2.[1,2] Nitrogen fertilizer demand will increase sharply as the human population increases in the future and will bring more challenges for energy and environmental protection. Plasma technology is evaluated as a potential alternative to produce nitrogen fertilizers.[3–5] Nitrate fertilizer could be effectively formed by air discharge in proper power consumption.[6–8] Moreover, this fertilizer is reported to have a low theoretical value of energy cost.[9] Meanwhile, ammonia emissions from the agroecological system are an important part of the global nitrogen cycle, causing a massive loss of crop nutrients and significantly affecting the environment and public health.[10,11] NH_3 is the main raw material of industrial

nitrogen fertilizer and is also the main pollutant for fog and haze formation.[12] China is the largest emitter of ammonia (NH_3) worldwide, and more than 80% of ammonia pollution in the air is from agriculture, mainly by the indiscriminate use of fertilizers and livestock manure.[13,14] A twofold benefit method for nitrogen fertilizer production and recycle is to use air discharge and wasted NH_3 to produce NH_4NO_3, which is predominantly used in agriculture as a high-nitrogen fertilizer, having a nitrogen content of 34%.[15] For example, this idea could be used in a farm when livestock manure is collected and a considerable amount of nitrogen fertilizer in the manure is lost through NH_3 volatilization. If the volatile parts of NH_3 can be captured by NO_x from air plasma to form NH_4NO_3 and return to the crops, there will be a significant contribution to both energy saving and environmental protection.[16,17]

The so-called "double nitrogen fertilizer" production requires investigating the reaction mechanism between the air plasma and ammonia. Existing reports on plasma interacting with NH_3 have mainly focused on using mild plasma to eliminate NH_3 in industrial waste gas/water directly.[18–20] Investigations on how to use air discharge and wasted NH_3 from farming system to form a double nitrogen fertilizer are rarely focused in the literature. Therefore, this study investigated, through direct image and Fourier-transform infrared spectroscopy (FTIR) observation, the reaction between the air plasma and NH_3 in three different reaction modes to reveal how the NH_4NO_3 could be effectively formed during the processes.

The plasma device used in this study was a needle–needle discharge driven by a DC power supply. The experimental setup is shown in Figure 1a. The pair of needles was made from stainless steel and mounted on the wall of a cubic chamber with a side length of 10 cm. One needle was connected to a high DC voltage, whereas the other was grounded. The distance between the two needle tips was fixed at 5 mm, and the vertical distance to the bottom was 3 cm. The applied voltage was measured by a high-voltage probe (Tektronix P6015A). A resistor ($R = 10\ \Omega$) was used in the circuit, and a differential probe (Tektronix P5200A) was used to measure the voltage V_r across the resistor. Therefore, the current in the circuit was calculated according to $I = V_r/R$. The air used in all the experiments was atmospheric air. The image of discharging in pure air is shown in Figure 1b. Brown gas (NO_2) was clearly observed inside the chamber when the discharge was on. Figure 1c shows the voltage and current waveforms in air discharge. The power consumed in the air discharge was calculated (22 W). A pair of ZnSe windows (15×2 mm) for FTIR measurements was mounted in parallel on the wall at the center of the chamber. The center of the widow was 2 cm above the needles. The gas could flow into the chamber through the hole at the bottom of the side wall and flow out the chamber through the hole at the top of the opposite side wall.

This study considered three modes of air plasma interaction with ammonia, as shown in Table 1. In Mode 1, for the first 5 min, the air discharge was ignited inside the chamber. After 5 min, the power was turned off, and NH_3

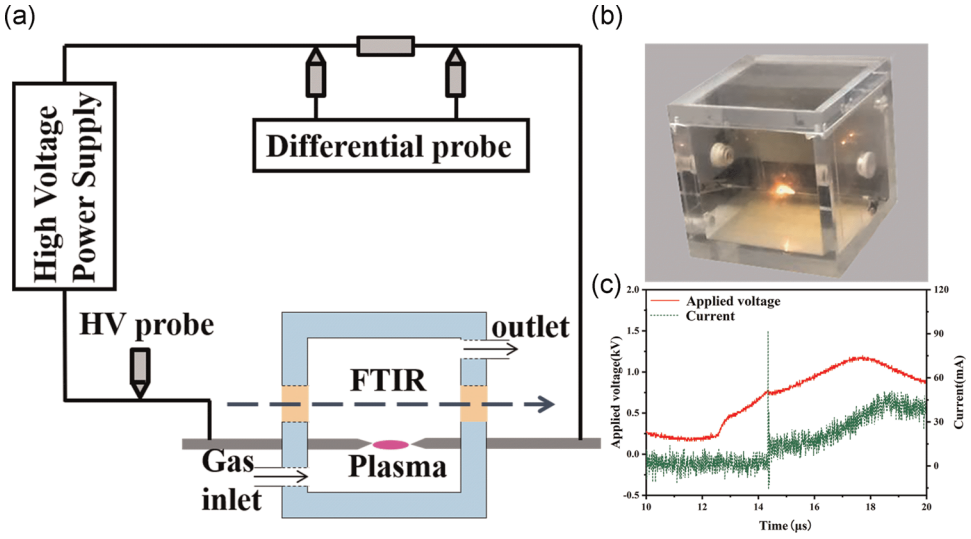

FIGURE 1 (a) Experimental setup; (b) image of the air discharge in the chamber; (c) voltage and current waveforms of air discharge. FTIR, Fourier-transform infrared spectroscopy; HV, high voltage

TABLE 1 Three reaction modes of plasma interaction with NH_3

Mode	Time (min)	
	0–5	6–10
1	Discharge in air	Discharge off and ammonia gas flows in
2	Discharge in air	Discharge and ammonia gas flows in
3	Discharge in a mixture of air and ammonia	

was introduced into the chamber at a flow rate of 80 ml/min. In Mode 2, the process of the first 5 min is similar to that in Mode 1. During the interval of 6–10 min, the difference was that the discharge was still on rather than turned off. In Mode 3, the discharge was ignited in a gas mixture of air and NH_3 and turned on during the entire process. The flow rates of the air and NH_3 were 500 and 80 ml/min, respectively. The electrical signals of discharging in Modes 2 and 3 were similar to that in Mode 1, and the power consumption was 24 and 26.5 W, respectively. The power consumption slightly increased when NH_3 was present in the working gas.

Subsequently, gas-phase FTIR spectra (vertex 70; Bruker) versus time were measured in different discharging gas and reaction modes to investigate the gas-phase chemical process during the reaction of air plasma and NH_3. Figure 2 shows the FTIR spectra of the different working gases and NO_x concentration of air discharge. Figures 2a and 2c show the typical gas-phase FTIR for the first 5 min in Mode 1/Mode 2 and Mode 3, respectively. When discharging in pure air, the typical peaks of NO (1800–1950 cm^{-1}), NO_2 (1550–1675 cm^{-1}), and HNO_3 (1200–1500 cm^{-1}) were observed. As clearly shown in the figure, the main products of air plasma were NO_x, and the concentration of the products increased with the discharging time. Figure 2b shows the NO and NO_2 quantitative concentration versus time. The NO and NO_2 concentration measured by FTIR was calibrated by using standard gas, and the calculated specific energy cost of nitrogen fixation here is ~150 GJ/tN. This specific energy cost is within the range reported by many other groups.[21–23] It is necessary to point out that due to the different calibration procedures in different labs and various databases used, the specific energy cost under similar conditions could vary a lot. In Figure 2c, when

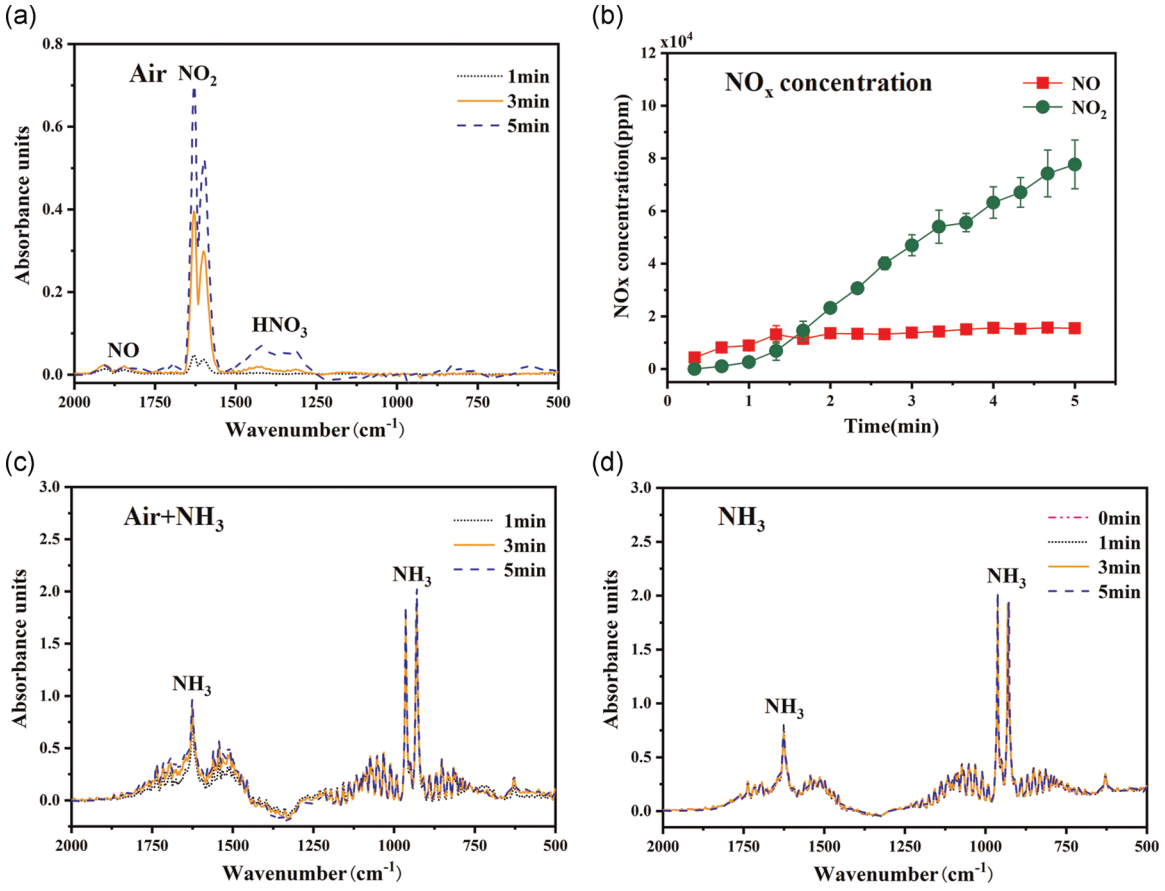

FIGURE 2 Gas-phase Fourier-transform infrared spectra in different discharging gases and NO_x concentration. (a) Air; (b) NO_x concentration; (c) air and NH_3; (d) NH_3

discharging in air and NH_3 mixture simultaneously, no NO or HNO_3 peaks were observed. The absorbance peak of NO_2 overlapped with that of NH_3, and the absorbance of these overlapped areas slightly increased with time. Figure 2d shows the gas-phase FTIR spectrum of NH_3 without/with discharge. Typical absorbance bands were present at 700–1300 and 1350–1900 cm^{-1}. The FTIR spectrum of pure NH_3 without discharge (0 min) was not different from that with discharge. Therefore, the slightly overlapped area increment in Figure 2c should be caused by NO_2 formation.

During the 6–10 min processes in the three modes, we continuously recorded the FTIR spectrums at different times. Figures 3a, 3b, 3c show the FTIR spectrum and the discharge chamber images after 10 min for Mode 1, Mode 2, and Mode 3, respectively. In Mode 1 (Figure 3a), a stable new peak at 1300–1500 cm^{-1} was observed during the interval of 6–10 min. This new

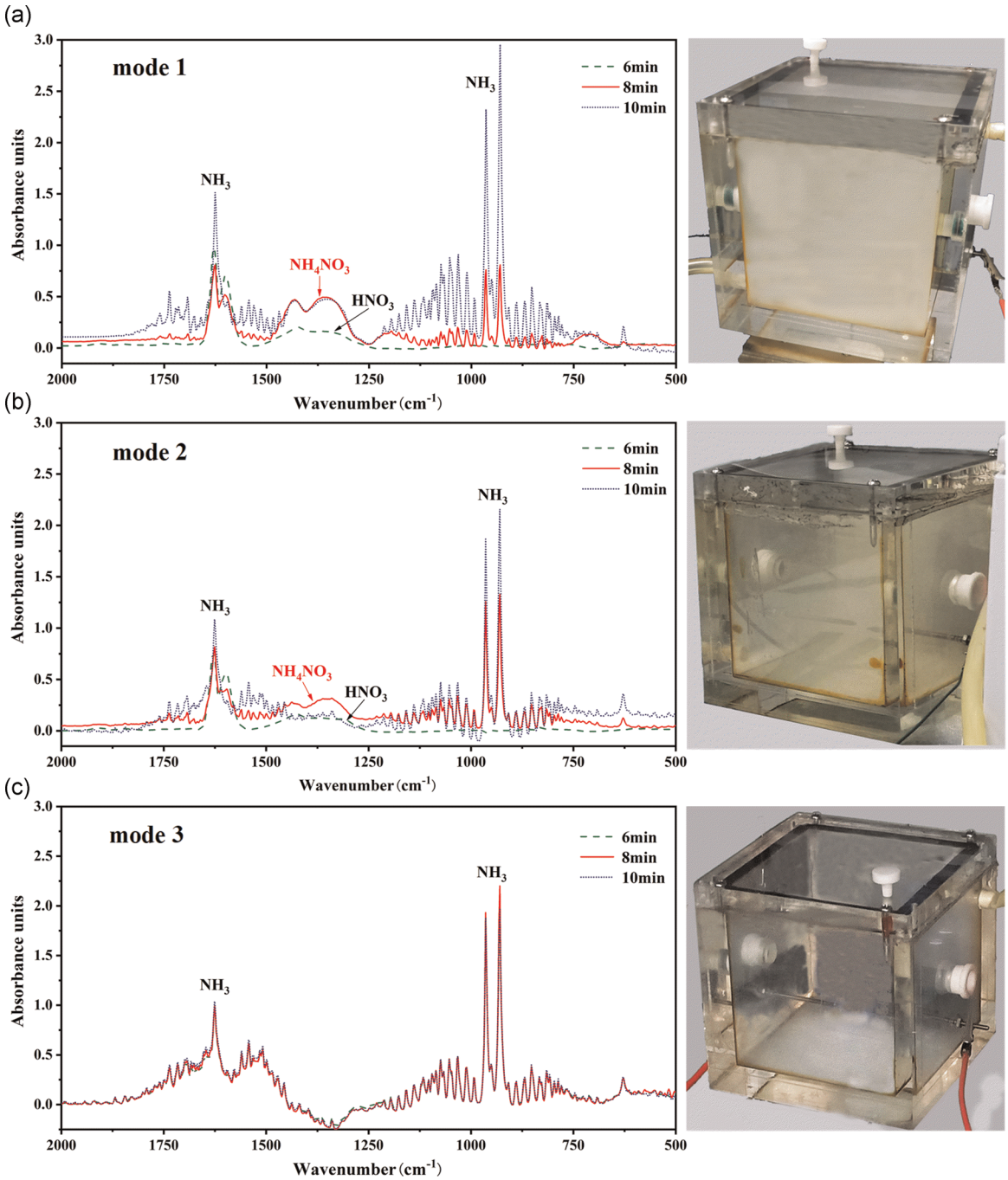

FIGURE 3 Gas-phase Fourier-transform infrared spectrum from 6- to 10-min process and images of new products' formation in the three reaction modes. (a) Mode 1; (b) mode 2; (c) mode 3

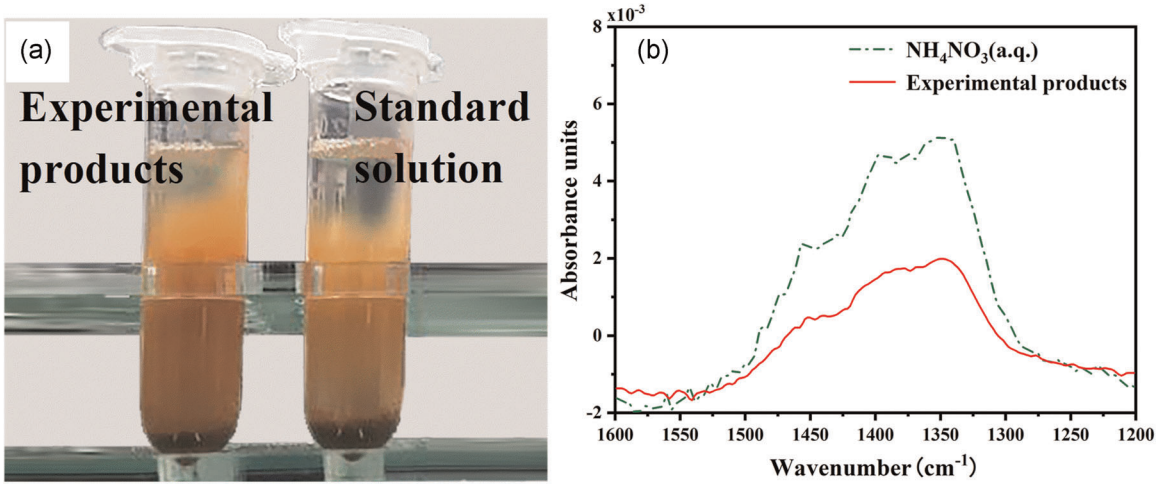

FIGURE 4 (a) White smoke identification by Nessler's reagent. The brown color indicates presence of NH_4^+ in the liquid; (b) attenuated total reflection–Fourier-transform infrared spectroscopy comparison of standard aqueous NH_4NO_3 and the experimental products

bond was identified as a typical NH_4NO_3 bond.[24] Meanwhile, a large amount of white smoke formation inside the chamber was observed, identified as NH_4NO_3 in the next section (Figure 4). As clearly shown in the figure, the absorbance of NO_2 decreased as NH_3 increased in the chamber from 6 to 10 min. NH_4NO_3 was formed in this reaction mode and remained stable. In Mode 2, the absorbance of NH_4NO_3 first increased, then decreased, and finally nearly disappeared at 10 min. The image of Mode 2 shows a relatively low concentration of white smog left inside the chamber at 10 min, compared with that in Mode 1. However, in Mode 3, when the plasma was always inside the chamber, we did not observe any new absorbance of NH_4NO_3 during the entire process. The image of the chamber in this mode remained transparent, and no white smoke was observed. It can be concluded that discharge affects the formation of NH_4NO_3.

The product was scraped from the inner wall of the reaction chamber after the experiment and then dissolved in 2-ml water for analysis. The aqueous phase of the product was analyzed using Nessler's reagent colorimetry (APS) and an ATR-FTIR spectrometer (vertex 70 equipped with a Platinum ATR sampling module; Bruker). The ammonium ion (NH_4^+) could react with Nessler's reagent to form a complex yellow sediment, whose color depth is related to the content of the ammonium ions. Figure 4a shows the image where Nessler's reagent detected the experimental products and standard NH_4Cl solution (0.1 mol/L). The brown color indicates that NH_4^+ was present in the product solution. Figure 4b shows the ATR-FTIR spectrum comparison between the standard aqueous NH_4NO_3 and the white smoke product. The standard NH_4NO_3 solution was substituted by mixing equal quantities of NH_4Cl and $NaNO_3$ at the same concentration in this investigation. The ATR-FTIR spectrum was completely matched and proved that the experimental product was NH_4NO_3.

We also measured the optical emission of the discharge and simulated the rotational temperature T_r of the discharge using the spectrum of the N_2 second positive system (result not shown here). The simulated T_r of the needle–needle DC arc discharge was approximately 2500 K. When the heat was transported to the entire chamber, the average temperature (approximately 3 cm away from the top center) measured by the thermocouple sensor was approximately 335 K and reached thermal equilibrium after 2 min. If the plasma is turned off after 5 min, the temperature inside the chamber will decrease to ~305 K at 10 min.

For the first 5 min, in Modes 1 and 2, NO_x was generated by the air discharge through the following reactions[25]:

$$N_2 + O \rightarrow NO + N, \quad (1)$$

$$N + O_2 \rightarrow NO + O, \quad (2)$$

$$H_2O + O \rightarrow OH + OH, \quad (3)$$

$$N_2 + OH \rightarrow NO + H, \quad (4)$$

$$O + NO + M \rightarrow NO_2 + M, \quad (5)$$

$$NO_2 + OH + N_2 \rightarrow HNO_3 + N_2. \quad (6)$$

In Mode 1, after 5 min, the discharge was turned off, and the average temperature inside the chamber was low. However, the temperature around the needle was still high and OH would still be possible to form through reaction (3). Some amount of HNO_3 could continue to be produced through reaction (6). NH_4NO_3 may be mainly formed through[25,26]

$$NH_3 + HNO_3 \rightarrow NH_4NO_3. \quad (7)$$

However, in Mode 2, the discharge was still on during 6–10 min; NH_4NO_3 may first be formed through reaction (7) because there were plenty of NO_x formed in the first 5 min. As the discharge continues, on the one hand, NH_4NO_3 may gradually undergo thermal decomposition through reactions (8–10), depending on the temperature.[15]

$$NH_4NO_3 \rightarrow NH_3 + HNO_3, \quad (8)$$

$$NH_4NO_3 \rightarrow N_2O + 2H_2O, \quad (9)$$

$$4NH_4NO_3 \rightarrow 3N_2 + 2NO_2 + 8H_2O. \quad (10)$$

On the other hand, similar to Mode 3, when discharging in air and NH_3, NH_3 would be decomposed by gas discharge through reaction (11) and consume OH through reaction (12). Meanwhile, NH_3 would also react with O to form NH_2 and OH (reaction 13) under DC air discharge.[27,28] The product NH_2 will rapidly consume NO through reaction (14), thus blocking the formation of NO_2 and HNO_3 and finally intercepting the formation of NH_4NO_3.[29]

$$NH_3 + N_2 \rightarrow NH_2 + H + N_2, \quad (11)$$

$$NH_3 + OH \rightarrow NH_2 + H_2O, \quad (12)$$

$$NH_3 + O \rightarrow NH_2 + OH, \quad (13)$$

$$NH_2 + NO \rightarrow N_2 + H_2O. \quad (14)$$

Other related reactions may also occur during these reaction modes, such as small amount of NH_3 formation during the process of plasma–water interaction[30,31] or the contribution of nitrogen excited species. However, we only listed some of the main possible reactions closely related to the NH_4NO_3 formation and dissociation here. Detailed reaction mechanism will be further studied in the next modeling work.

In conclusion, three modes of air plasma interaction with NH_3 for the NH_4NO_3 formation were investigated. NH_4NO_3 could be stably formed by directly mixing gas-phase NO_x products from air plasma and NH_3 with plasma off. Discharging in the air/NO_x/NH_3 mixture affects the NH_4NO_3 formation process. The gas discharge may block the formation of NH_4NO_3 through a direct thermal decomposition process and an indirect NH_3 decomposition with NO/OH consumption. Future works should be performed on detailed chemical kinetic studies, quantitative measurements, and numerical calculations to further understand the mechanism and optimize the conditions.

ACKNOWLEDGMENT

The authors are grateful for financial support from the Independent Innovation Fund of Huazhong University of Science and Technology (No. 2018KFYYXJJ071).

DATA AVAILABILITY STATEMENT

The data that supports the findings of this study are available within the article.

ORCID

Zilan Xiong http://orcid.org/0000-0003-1095-3959

REFERENCES

[1] R. R. Schrock, *Proc. Natl. Acad. Sci. U. S. A.* **2006**, *103*, 17087.
[2] C. J. Dawson, J. Hilton, *Food Policy* **2011**, *36*, S14.
[3] J. G. Chen, R. M. Crooks, L. C. Seefeldt, K. L. Bren, R. M. Bullock, M. Y. Darensbourg, P. L. Holland, B. Hoffman, M. J. Janik, A. K. Jones, M. G. Kanatzidis, P. King, K. M. Lancaster, S. V. Lymar, P. Pfromm, W. F. Schneider, R. R. Schrock, *Science* **2018**, *360*, eaar6611.
[4] X. Hu, X. Zhu, X. Wu, Y. Cai, X. Tu, *Plasma Processes Polym.* **2020**, *17*, e2000072.
[5] N. C. Roy, C. Pattyn, A. Remy, N. Maira, F. Reniers, *Plasma Processes Polym.* **2020**, *18*, e2000087.
[6] B. S. Patil, Q. Wang, V. Hessel, J. Lang, *Catal. Today* **2015**, *256*, 49.
[7] W. Wang, B. Patil, S. Heijkers, V. Hessel, A. Bogaerts, *ChemSusChem* **2017**, *10*, 2110.
[8] X. Pei, D. Gidon, Y.-J. Yang, Z. Xiong, D. B. Graves, *Chem. Eng. J.* **2019**, *362*, 217.
[9] N. Cherkasov, A. O. Ibhadon, P. Fitzpatrick, *Chem. Eng. Process.* **2015**, *90*, 24.
[10] J. X. Warner, R. R. Dickerson, Z. Wei, L. L. Strow, Y. Wang, Q. Liang, *Geophys. Res. Lett.* **2017**, *44*, 2875.
[11] J. Lelieveld, J. S. Evans, M. Fnais, D. Giannadaki, A. Pozzer, *Nature* **2015**, *525*, 367.
[12] B. Gu, M. A. Sutton, S. X. Chang, Y. Ge, J. Chang, *Front. Ecol. Environ.* **2014**, *12*, 265.
[13] X. Zhang, Y. Wu, X. Liu, S. Reis, J. Jin, U. Dragosits, M. Van Damme, L. Clarisse, S. Whitburn, P. F. Coheur, B. Gu, *Environ. Sci. Technol.* **2017**, *51*, 12089.
[14] Y. Wu, X. Xi, X. Tang, D. Luo, B. Gu, S. K. Lam, P. M. Vitousek, D. Chen, *Proc. Natl. Acad. Sci. U. S. A.* **2018**, *115*, 7010.
[15] K.-H. Zapp, K.-H. Wostbrock, M. Schäfer, K. Sato, H. Seiter, W. Zwick, R. Creutziger, H. Leiter, in *Ullmann's Encyclopedia of Industrial Chemistry*, Wiley-VCH Verlag GmbH & Co. KGaA, Weinheim, Germany **2000**.
[16] D. B. Graves, L. B. Bakken, M. B. Jensen, R. Ingels, *Plasma Chem. Plasma Process.* **2019**, *39*, 1.
[17] R. Ingels, D. B. Graves, *Plasma Med* **2015**, *5*, 257.
[18] L. Xia, L. Huang, X. Shu, R. Zhang, W. Dong, H. Hou, *J. Hazard. Mater.* **2008**, *152*, 113.
[19] B. G. Nazarenko, O. B. Shubin, in *Proc. Second Environ. Phys. Conf.* **2007**, Alexandria, Egypt.
[20] J. J. Ruan, W. Li, Y. Shi, Y. Nie, X. Wang, T. E. Tan, *Chemosphere* **2005**, *59*, 327.
[21] M. A. Malik, *Plasma Chem. Plasma Process.* **2016**, *36*, 737.
[22] Y. Wang, A. W. DeSilva, G. C. Goldenbaum, R. R. Dickerson, *J. Geophys. Res.-Atmos.* **1998**, *103*, 19149.
[23] B. S. Patil, J. R. Palau, V. Hessel, J. Lang, Q. Wang, *Plasma Chem. Plasma Process.* **2016**, *36*, 241.
[24] H. B. Wu, M. N. Chan, C. K. Chan, *Aerosol. Sci. Technol.* **2007**, *41*, 581.

[25] D. L. Baulch, C. T. Bowman, C. J. Cobos, R. A. Cox, T. Just, J. A. Kerr, M. J. Pilling, D. Stocker, J. Troe, W. Tsang, R. W. Walker, J. Warnatz, *J. Phys. Chem. Ref. Data* **2005**, *34*, 757.
[26] J. H. Lee, S. I. Lee, O. C. Kwon, *Int. J. Hydrogen Energy* **2010**, *35*, 11332.
[27] P. Sabia, M. V. Manna, A. Cavaliere, R. Ragucci, M. de Joannon, *Fuel* **2020**, *276*, 118054.
[28] J. Chen, W. Fan, X. Wu, S. Liu, H. Guo, Z. Liu, X. Wang, *Fuel* **2021**, *283*, 119335.
[29] J. Park, M. C. Lin, *J. Phys. Chem. A* **1999**, *103*, 8906.
[30] Y. Gorbanev, E. Vervloessem, A. Nikiforov, A. Bogaerts, *ACS Sustain. Chem. Eng.* **2020**, *8*, 2996.
[31] J. R. Toth, N. H. Abuyazid, D. J. Lacks, J. N. Renner, R. M. Sankaran, *ACS Sustain. Chem. Eng.* **2020**, *8*, 14845.

How to cite this article: Y. Zhu, Z. Xiong, M. Li, X. Chen, C. Lu, Z. Zou, *Plasma Processes Polym.* **2021**, e2000223. https://doi.org/10.1002/ppap.202000223